Grain boundaries in vortex matter

Paolo Moretti,[1] M.-Carmen Miguel,[2] and Stefano Zapperi[3,4]
[1]*Center for Materials Science and Engineering, University of Edinburgh, King's Buildings, Sanderson Building, Edinburgh EH9 3JL, United Kingdom*
[2]*Departament de Física Fonamental, Facultat de Física, Universitat de Barcelona, Avinguda Diagonal 647, E-08028, Barcelona, Spain*
[3]*INFM UdR Roma 1 and SMC, Dipartimento di Fisica, Università "La Sapienza," P. le A. Moro 2, 00185 Roma, Italy*
[4]*Istituto dei Sistemi Complessi, CNR, via dei Taurini 19, 00185 Roma, Italy*
(Received 16 December 2004; revised manuscript received 14 April 2005; published 5 July 2005)

We explore the statistical properties of grain boundaries in the vortex polycrystalline phase of type-II superconductors. Treating grain boundaries as arrays of dislocations interacting through linear elasticity, we show that self-interaction of a deformed grain boundary is equivalent to a nonlocal long-range surface tension. This affects the pinning properties of grain boundaries, which are found to be less rough than isolated dislocations. The presence of grain boundaries has an important effect on the transport properties of type-II superconductors as we show by numerical simulations: our results indicate that the critical current is higher for a vortex polycrystal than for a regular vortex lattice. Finally, we discuss the possible role of grain boundaries in vortex lattice melting. Through a phenomenological theory we show that melting can be preceded by an intermediate polycrystalline phase.

DOI: 10.1103/PhysRevB.72.014505 PACS number(s): 74.25.Qt, 61.72.Mm

I. INTRODUCTION

The phase diagram of high-temperature superconductors is an object of active investigation in condensed matter physics. Most high-T_c materials behave in a magnetic field as type-II superconductors, with further complications due to the broader phase space—in terms of temperature T and field H—in comparison to conventional type-II superconductors.[1–3] This leads to several possibilities for the mixed phase, where magnetic flux penetration is incomplete. As first discussed by Abrikosov for conventional superconductors,[4] flux is quantized and carried by vortex lines which are arranged in the form of a lattice. As in conventional matter strong enough fluctuations destroy long-range order: when temperature is raised the vortex lattice melts into a vortex liquid.[5–7] Fluctuations are also provided by quenched disorder that is intrinsically present in these materials, leading to complex glassy phases.[8–13]

While several experimental methods have been used to investigate vortex matter, a direct image of the geometrical and topological properties of the vortices can be obtained by the Bitter decoration technique.[14] Its application to conventional superconductors provided the first direct proof of the vortex lattice[15] predicted by Abrikosov.[4] The observed lattice contains, however, topological defects, such as dislocations and grain boundaries. These last extended defects are the signature of a vortex polycrystal with crystalline grains of different orientations.[14,16] Vortex polycrystals have been observed, after field cooling, in various superconducting materials such as NbMo,[14,16] $NbSe_2$,[17–20] BSCCO,[21] and YBCO.[22] The grain size is typically found to grow with applied magnetic field.[16,17] Moreover, two-sided decoration experiments show that the grain boundaries thread the sample from top to bottom,[17,18] i.e., one observes a columnar grain structure. Despite the wealth of experimental observations, there is no detailed theory accounting for the formation of vortex polycrystals.

The behavior of vortex matter in presence of disorder represents a formidable theoretical problem that has still not been completely solved. While early theoretical considerations seemed to imply that even a small amount of disorder would lead to the loss of long-range order[23] and to the formation of an amorphous vortex glass phase,[11] it is now accepted that at low disorder vortices arrange into a topologically ordered phase: the Bragg glass.[13,24] The existence of this phase, characterized by logarithmically growing correlations, slow relaxation, and other glassy features, has been now experimentally confirmed.[25] At high enough disorder, the Bragg glass phase is found to be unstable against dislocation proliferation and one may expect the transition into an amorphous vortex glass.[26–28] The precise nature of this transition and, more generally, the mechanism underlying vortex lattice melting is still under debate. Typical melting theories are based on variants of the Lindemann criterion with disorder,[29] or involve dislocation proliferation mechanisms.[30]

The properties of dislocations in the vortex lattice have been the object of extensive theoretical investigations,[31–34] but grain boundaries are less studied although they are often observed in numerical simulations.[35–37] For instance, the vortex plastic flow in the Corbino disk geometry is characterized by radial grain boundaries sliding in the tangential direction.[35] In addition, recent numerical simulations indicate the presence of an intermediate polycrystalline phase before the melting transition.[36,37] This behavior was observed using different numerical methods in two dimensions[36] and in presence of columnar disorder.[37] This suggests that, in some conditions, grain boundaries may play a role in the melting process, as in the theory of grain-boundary-induced melting of two-dimensional crystals.[38]

Here we analyze the properties of grain boundaries in vortex matter describing the fluctuations induced by disorder, stress, or temperature. A grain boundary can be considered as an array of dislocations, whose dynamics is ruled by internal stresses. While ideally a grain boundary minimizes its energy

by remaining flat, the action of external perturbations leads to deformations that can be described by the theory of elasticity.[39] We compute the self-interaction of a deformed grain boundary extending the results obtained for isotropic elasticity[39] to the case of the vortex lattice. Grain boundaries are much stiffer than isolated dislocations, possessing a nonlocal long-range surface tension and, in presence of disorder, they are expected to be less rough than isolated dislocations. We estimate the grain boundary roughness exponent using the random stress model introduced in Ref. 34 for vortex dislocations. Using scaling arguments, we also derive the creep law for thermally activated motion and discuss disorder-arrested grain growth.[40]

The critical current is an important property of type-II superconductors, since it represents the current below which vortices are pinned and the material conducts without resistance. It is thus interesting to understand how the topological properties of vortex matter influence its behavior. We use numerical simulations of interacting vortices to quantify the effect of grain boundaries on the critical current. We obtain a polycrystalline vortex structure by relaxing at zero temperature a random initial vortex arrangement. This process simulates a typical field-cooling experiment in which the temperature is rapidly decreased from above T_c in the presence of a field. The system moves rapidly toward lower-energy configurations corresponding to zero temperature and thermal effects can thus be disregarded. In this case magnetic flux is present in the material as it enters the superconducting phase and vortices are initially disordered. Once grain growth has stopped, we simulate the effect of an external current flowing through the sample by applying a constant Lorenz force. The critical current is then defined as the current at which vortices start to move steadily. By repeating the simulations for different values of the vortex number, representing the effect of various magnetic field intensities, we show that the critical current for a polycrystal is always larger than the one obtained for a perfect lattice. This reflects the fact that a polycrystalline assembly is more effectively pinned than a perfect lattice because it can accommodate better in the disordered landscape. In addition, we find that the corresponding *IV* curve is hysteretic upon ramping up and down the current. This result can explain the difference in transport properties between field-cooled and zero-field-cooled samples and the related hysteresis commonly measured experimentally.[10,41–46]

Finally, we discuss the possible role of grain boundary in vortex lattice melting by constructing a free-energy functional for the grain boundary density along the lines of Ref. 38. We derive the contribution due to grain boundary fluctuations and junction formation and show the presence of a polycrystalline phase with a finite grain boundary density. As temperature is increased the grain boundary density increases and the system melts. The theory predicts a value for the melting temperature that is quite similar to that obtained in Ref. 30 considering only the contribution of isolated dislocations. We notice that the presence of an intermediate polycrystalline phase in vortex lattice melting was recently proposed on a phenomenological basis in Ref. 47 and experimental evidence was reported for $La_{1.9}Sr_{0.1}CuO_4$.[48]

The paper is organized as follows. In Sec. II we compute the self-energy of a deformed vortex grain boundary. In Sec. III we analyze the interaction between grain boundaries and disorder, as well as its relevance for pinning, creep, and grain growth. Section IV reports the results of numerical simulations of interacting vortices where we discuss the effect of grain boundaries on the critical current. In Sec. V we discuss the role of grain boundaries in the melting process through a phenomenological theory. Section VI is devoted to conclusions. Finally, the Appendix reports details of the derivation reported in Sec. V.

II. ELASTICITY OF GRAIN BOUNDARIES

A simplified but rather effective description of the vortex lattice is provided by its representation as an elastic crystal of flux lines. At large enough distances, the elastic energy of the vortex lattice can be expressed in terms of the vortex displacement field $\mathbf{u}$ as follows:

$$\mathcal{H} = \frac{1}{2}\int d^3r[c_{66}(\boldsymbol{\nabla}\mathbf{u})^2 + (c_{11}-c_{66})(\boldsymbol{\nabla}\cdot\mathbf{u})^2 + c_{44}(\partial_z\mathbf{u})^2], \tag{1}$$

where c_{11}, c_{44}, c_{66} are the local elastic moduli, and the magnetic induction $\mathbf{B}$ is parallel to the z direction. Within this representation, we shall introduce an ideal low-angle grain boundary as an infinite periodic array of straight dislocations in the vortex lattice oriented along the z axis, spatially arranged along the y axis with an array spacing equal to D, and with Burgers vectors $\mathbf{b}$ pointing along the x direction (i.e., edge dislocations). The wandering of the ith dislocation line can be schematized through the vector $\mathbf{R}_i(z)=(X_i+X_i(z), iD)$, assuming that all displacements take place within glide planes, i.e., the xz plane, so that $X_i+X_i(z)$ plays the role of the displacement field of the grain boundary as well. X_i is a constant term and deals with rigid displacements of the dislocation lines. Its contribution to the elastic Hamiltonian is known since it is the same as for straight dislocations in isotropic lattices.[39] In the following this contribution will be referred to as $\mathcal{H}_0$.

Defining $\mathbf{r}_\perp=(x,y)$, the vector $\mathbf{u}$ can be decomposed as $\mathbf{u}(\mathbf{r})=\mathbf{u}^r(\mathbf{r}_\perp,z)+\Sigma_i\mathbf{u}_i^s(\mathbf{r}_\perp-\mathbf{R}_i(z),z)$, where $\mathbf{u}_i^s(\mathbf{r}_\perp-\mathbf{R}_i(z),z)$ is the singular solution of the two-dimensional problem for each value of z

$$c_{66}\boldsymbol{\nabla}^2\mathbf{u}_i^s + (c_{11}-c_{66})\,\boldsymbol{\nabla}\,(\boldsymbol{\nabla}\cdot\mathbf{u}_i^s) = 0,$$

$$\oint d\mathbf{u}_i^s = \mathbf{b}_i \quad \forall\, i,z \tag{2}$$

while $\mathbf{u}^r(\mathbf{r}_\perp,z)$ is the regular part of the solution due to the interplane couplings along z.

Minimizing Eq. (1) with respect to $\mathbf{u}$ and imposing the first expression of Eqs. (2) we find the differential equation

$$c_{66}\boldsymbol{\nabla}^2\mathbf{u}^r + (c_{11}-c_{66})\,\boldsymbol{\nabla}\,(\boldsymbol{\nabla}\cdot\mathbf{u}^r) + c_{44}\partial_z^2\mathbf{u}^r = -c_{44}\partial_z^2\sum_i \mathbf{u}_i^s, \tag{3}$$

where the field $\mathbf{u}_i^s$ on the right-hand side term of the equation is known from elasticity theory as the displacement field

generated by a point edge dislocation at $\mathbf{R}_i(z)$. Performing a first-order expansion in the displacement $X_i+X_i(z)$, the derivative removes any dependence on the constant part X_i, and we can rewrite Eq. (3) in Fourier space as follows:

$$c_{66}q^2\mathbf{u}^r + (c_{11}-c_{66})\mathbf{q}(\mathbf{q}\cdot\mathbf{u}^r) + c_{44}k_z^2\mathbf{u}^r = c_{44}\frac{k_z^2}{q^2}\mathbf{A}, \quad (4)$$

where $\mathbf{q}=(k_x,k_y)$ and

$$\mathbf{A} = \sum_n e^{ik_yY_n}X_n(k_z)\times\begin{pmatrix} k_y[r-(1-r)\cos 2\phi] \\ k_x[r+(1-r)\cos 2\phi]\end{pmatrix} \quad (5)$$

with $r=c_{66}/c_{11}$, $\cos\phi=k_x/k$, and $\sin\phi=k_y/k$.

$\mathbf{A}$ can be decomposed in its longitudinal and transverse components $\mathbf{A}_L=\mathbf{q}(\mathbf{q}\cdot\mathbf{A})/q^2$ and $\mathbf{A}_T=\mathbf{A}-\mathbf{A}_L$. The Hamiltonian (1) thus becomes

$$\mathcal{H} = \mathcal{H}^0 + \frac{1}{2}c_{44}b^2\sum_{n,m}\int\frac{d^2q}{(2\pi)^2} \times\int\frac{dk_z}{2\pi}k_z^2M(q,\phi,k_z)e^{ik_y(n-m)D}X_n(k_z)X_m(-k_z) \quad (6)$$

where we have neglected constant terms and defined

$$M(q,\phi,k_z)\equiv\left[\frac{c_{66}\cos^2 2\phi}{c_{66}q^2+c_{44}k_z^2}+\frac{c_{11}r^2\sin^2 2\phi}{c_{11}q^2+c_{44}k_z^2}\right]. \quad (7)$$

Defining $X_n(k_z)=\int_{\mathrm{BZ}}(dQ_y/2\pi)e^{-iQ_ynD}X(Q_y,k_z)$, where the integral is restricted to the first Brillouin zone (BZ), we get

$$\mathcal{H} = \frac{1}{2}c_{44}\frac{b^2}{D^2}\sum_{G_y}\int_{\mathrm{BZ}}\frac{dQ_y}{2\pi}\int\frac{dk_z}{2\pi}\Xi(Q_y+G_y,k_z) \times X(Q_y,k_z)X(-Q_y,-k_z) \quad (8)$$

where we have introduced the interaction kernel

$$\Xi(Q_y+G_y,k_z) = k_z^2\int_{-\infty}^{+\infty}M(k_x,Q_y+G_y,k_z)dk_x \quad (9)$$

with

$$M(k_x,k_y,k_z) = \frac{(k_x^2-k_y^2)^2}{(k_x^2+k_y^2)^2[k_x^2+k_y^2+(c_{44}/c_{66})k_z^2]} + 4r^2\frac{k_x^2k_y^2}{(k_x^2+k_y^2)^2[k_x^2+k_y^2+(c_{44}/c_{11})k_z^2]}. \quad (10)$$

Solving the integral in Eq. (9) leads to

$$\mathcal{H} = \mathcal{H}^0 + \frac{\pi b^2}{2D^2}\frac{c_{66}^2}{c_{44}}\sum_{G_y}\int_{\mathrm{BZ}}\frac{dQ_y}{2\pi}\int\frac{dk_z}{2\pi}X(Q_y,k_z)X(-Q_y,-k_z) \times\frac{1}{k_z^2}\left[\frac{[2k_y^2+(c_{44}/c_{66})k_z^2]^2}{\sqrt{k_y^2+(c_{44}/c_{66})k_z^2}}-4k_y^2\sqrt{k_y^2+\frac{c_{44}}{c_{11}}k_z^2} -2\left(\frac{c_{44}}{c_{66}}-\frac{c_{44}}{c_{11}}\right)|k_y|k_z^2\right] \quad (11)$$

with $k_y=Q_y+G_y$, $c_{44}/c_{66}\gg 1$, and $c_{44}/c_{11}\sim 1$.

Moreover, keeping the leading term of the right-hand side in Eq. (11) we get

$$\mathcal{H}_{GB} = \frac{\pi b^2}{2D^2}\sum_{G_y}\int\frac{dQ_y}{2\pi}\int\frac{dk_z}{2\pi}(2c_{66}|k_y| + \sqrt{c_{44}c_{66}}|k_z|)X(k_y,k_z)X(-k_y,-k_z). \quad (12)$$

It is a common procedure to rescale the y coordinate by a factor $\frac{1}{2}\sqrt{c_{44}/c_{66}}$,[1] in order to get an isotropic reference frame. The elastic Hamiltonian thus becomes

$$\mathcal{H} = K\frac{\pi b^2}{2D^2}\sum_{G_y}\int\frac{d^2k}{(2\pi)^2}|\mathbf{k}|X(\mathbf{k})X(-\mathbf{k}), \quad (13)$$

where $\mathbf{k}=(k_y,k_z)$ and $K=\sqrt{c_{44}c_{66}}$.

In this limit, the same result predicted by the isotropic theory[39] is thus obtained. The nonlocal character of the elastic kernel ($\propto k$) manifests that long-range interactions between dislocations stiffen the grain boundary, and that a surface tension approximation is not suitable for a correct description of its elastic properties.

III. INTERACTION BETWEEN GRAIN BOUNDARIES AND DISORDER

A. Random stresses

Point defects such as vacancies or interstitials in the underlying crystalline structure of the superconducting material, and/or substitutional impurities, etc., act as pinning centers for the magnetic vortices. For weak pinning forces, disorder can be theoretically described by a *random pinning potential* acting directly on flux lines. The distortions generated in the vortex lattice as well as the occurrence of depinning under an applied current have been intensively studied over the last decades (for a review see Ref. 1).

Here, we are instead concerned with the behavior of grain boundaries in presence of disorder. The disorder-induced vortex lattice displacement field gives rise to shear elastic stresses, which, in turn, generate Peach-Koehler forces on the vortex lattice dislocations.[49] In other words, as the final consequence of these disorder-induced distortions, there is an effective pinning stress field $\sigma_{ij}(\mathbf{r})$ acting as well on vortex dislocations (and therefore on grain boundaries). The statistical properties of the random stress field have been analyzed in Ref. 34 in the case of vortex dislocations. In the following, we recall their derivation and adapt it to the case of grain boundaries.

On short length scales, where vortex displacements $\mathbf{u}(\mathbf{r})$ are smaller than the coherence length ξ (the so-called Larkin regime[50]), a perturbative calculation can be performed. As discussed in Ref. 30, for grain boundaries it is necessary to consider larger scales, $\xi<u<a$, where vortices are well described by a *random manifold* (RM) model[1,13] in which flux lines are subject to an uncorrelated pinning potential. In this case, the relative displacements correlation function is

$$B_{ij}(\mathbf{r}-\mathbf{r}') = \overline{[u_i(\mathbf{r})-u_i(\mathbf{r}')][u_j(\mathbf{r})-u_j(\mathbf{r}')]} \simeq a^2\left(\frac{r-r'}{R_a}\right)^{2\zeta_{RM}}. \quad (14)$$

Here R_a is the crossover length, also known as the *positional correlation length*, at which average vortex displacements are of the order of a. The roughness exponent can be estimated as $\zeta_{RM} \approx 1/5$.

On scales larger than R_a, vortex displacements are of the order of a and the periodicity of the lattice comes into play.[13] Displacements are shown to grow logarithmically, with correlations of the form $B(\mathbf{r}-\mathbf{r}') \simeq (a/\pi)^2 \ln(e|r-r'|/R_a)$, and topological defects are absent. This quasiordered phase is known as the *Bragg glass* (BrG).[13]

The defect-free regions discussed above act on vortex lattice dislocations through a Peach-Koehler stress field.[49] Statistical properties of this stress field can be obtained from the correlator $B_{ij}(\mathbf{r}-\mathbf{r}')$ applying linear elasticity theory. In particular, the stress correlator $S_{xy}(\mathbf{r}-\mathbf{r}') = \overline{\sigma_{xy}(\mathbf{r})\sigma_{xy}(\mathbf{r}')}$ will read

$$S_{xy}(\mathbf{r}-\mathbf{r}') = (K^2/2)[\partial_x \partial_{x'} B_{yy}(\mathbf{r}-\mathbf{r}') + \partial_y \partial_{y'} B_{xx}(\mathbf{r}-\mathbf{r}') + 2\partial_x \partial_{y'} B_{yx}(\mathbf{r}-\mathbf{r}')]. \quad (15)$$

Replacing previous expressions of $B_{ij}(\mathbf{r}-\mathbf{r}')$ we easily obtain the stress fluctuations over a distance R,

$$S_{xy}(R) \approx K^2 \frac{a^2}{R^2} \begin{cases} (R/R_a)^{2\zeta_{RM}}, & R < R_a, \\ 1, & R > R_a, \end{cases} \quad (16)$$

where the first case applies to the RM description, while the second corresponds to the BrG regime. The effect of this random stress on isolated dislocations was studied in Ref. 34 where several differences with respect to the case of vortex lines were pointed out. Here we consider the behavior of grain boundaries, expecting substantially different features arising from long-range interactions between grain boundary dislocations.

The Hamiltonian of a grain boundary in the presence of disorder can be written as

$$\mathcal{H}_d = \mathcal{H} + \mathcal{H}_{pin}, \quad (17)$$

with $\mathcal{H}$ being the elastic term calculated above and $\mathcal{H}_{pin}$ the pinning term given by

$$\mathcal{H}_{pin} = \sum_i \int dz\, X_i(z) b \sigma_{xy}[X_i(z), iD, z]. \quad (18)$$

Although there is no explicit expression for $\mathcal{H}_{pin}$, it is possible to derive its fluctuations over a distance L as

$$E_{pin}^2 = b^2 \sum_{i,i'} \int_0^L dz \int_0^L dz' X_i(z) X_{i'}(z') \times \overline{\sigma_{xy}[X_i(z), iD, z]\sigma_{xy}[X_{i'}(z'), i'D, z']}. \quad (19)$$

Taking the continuum limit of the sum and integrating for both the RM and the BrG regimes, the typical pinning energy when displacing a grain boundary segment of length L by an amount $\overline{X_i^2}^{1/2} \sim u_{GB}$ will be thus given by

$$E_{pin}^2 \simeq \left(\frac{Kab}{D}\right)^2 L^2 u_{GB}^2 \begin{cases} \left(\frac{L}{R_a}\right)^{2/5} & \text{(RM)} \\ \ln \frac{L}{u_{GB}} & \text{(BrG)} \end{cases} \quad (20)$$

A dimensional estimate of the elastic cost of fluctuations of a grain boundary fraction of linear dimension L has the form

$$E_{el} = \frac{Kb^2}{D^2} L u_{GB}^2. \quad (21)$$

Since we are dealing with static properties of the system, we can impose equilibrium conditions balancing E and E_{pin}, that is, equating the elastic cost of fluctuations and the energy gain due to the interaction with disorder. Defining the roughness exponent of a grain boundary ζ_{GB} from $u_{GB}^2 \sim L^{2\zeta_{GB}}$ we get

$$\zeta_{GB} \approx \begin{cases} \frac{1}{5} & \text{(RM)}, \\ \log^{1/2} & \text{(BrG)}. \end{cases} \quad (22)$$

The long-range stiffness of a grain boundary reduces the values of roughness exponents in comparison with the case of isolated dislocations.[34]

B. Depinning and creep

So far we have not considered the effect of driving forces on the dislocation arrangement. Driving forces for grain boundary motion can be externally induced by a current flowing in the superconductor or internally generated by the ordering process during grain growth.[51] In both cases, the presence of a driving shear stress σ gives rise to a Peach-Koehler force per unit length of the form $F_{drive} = \sigma b$ acting on each dislocation along the grain boundary fraction considered or, in other words, to a total driving force per unit length equal to $F_{drive} = \sigma b L/D$.

At low stress grain boundaries are pinned. One can estimate the depinning stress from conventional scaling arguments. The energy associated with the driving force acting on a low-angle grain boundary segment of length L and displaced by an amount u_{GB} is given by

$$E_{drive}(L) = \sum_i \int dz\, F_{drive}^i(z) u_{GB}(y_i, z) \sim \frac{\sigma b L^2}{D} u_{GB}. \quad (23)$$

The depinning stress can be obtained by comparing this driving term with the pinning energy reported in Eq. (20). The relevant scale to consider is due to the interplay between elasticity and disorder and results from the minimization of $E_{el} + E_{pin}$ for displacements of the order of $u_{GB} \simeq a \simeq b$, corresponding to the dislocation core. A similar approach is followed in the case of vortices,[50] which are pinned for displacements of the order of ξ, the size of the vortex core and, hence, the relevant scale for the interaction with impurities. In our case, we obtain the Larkin length as $L_p \simeq (b/D)^5 R_a$, which is typically smaller than R_a. The depinning stress is then identified as the stress necessary to depin a section of dimension L_p:

$$\sigma_c \simeq Kb^2/(DL_p) = KD^4/(b^3 R_a). \quad (24)$$

TABLE I. Comparison between roughness and creep exponents calculated for isolated dislocations, 2D dislocation bundles (Ref. 34), and low-angle grain boundaries, taking into account nonlocal effects proven in Sec. II.

Exponent	Length scale	Isolated dislocation	2D bundle	Grain boundary
ζ	RM	15/13	5/13	1/5
ζ	BrG	$1-\log^{2/3}$	1/3	$\log^{1/2}$
μ	RM	17/11	10/21	7/4
μ	BrG	1	2/5	1

For low values of the stress ($\sigma \ll \sigma_c$), the response of a grain boundary is mainly due to thermally activated motion in a disordered environment.[1] In this case, we expect a highly nonlinear creep motion with an average velocity $v \sim \exp[-C(\sigma_c/\sigma)^{\mu}/T]$, where C is a constant, and μ is the creep exponent that quantifies the divergence of the energy barriers $U(\sigma) \sim \sigma^{-\mu}$ separating metastable states. An estimation of the exponent μ for a grain boundary can be obtained from a simple dimensional scaling argument, which is confirmed by a more rigorous renormalization group analysis. The typical energy barrier for a grain boundary section of length L is of the order of $U(L) \sim L^{1+2\zeta_{GB}}$, where we have used $u_{GB} \sim L^{\zeta_{GB}}$. In presence of an applied stress σ, we can compute the typical grain boundary length $L(\sigma)$ involved in thermal activated motion minimizing $U(L)+E_{drive}(L)$. The result yields $L(\sigma) \sim \sigma^{1/(\zeta_{GB}-1)}$. Using this length, we obtain that the typical energy barrier depends on the stress as

$$U(\sigma) \sim \sigma^{(1+2\zeta_{GB})/(\zeta_{GB}-1)}, \tag{25}$$

implying that $\mu = 2\zeta_{GB}/(2-\zeta_{GB})$. For the RM and BrG regimes the exponents are given by

$$\mu_{pl} \approx \begin{cases} \frac{7}{4} & \text{(RM)}, \\ 1 & \text{(BrG)}. \end{cases} \tag{26}$$

Now these exponents are larger than their counterparts calculated for isolated dislocations. In other words, the formation of grain boundaries affects vortex dynamics lowering ordinary creep rates. On Table I, all previous results are summarized and compared to estimates for different dislocation arrays.

C. Grain growth

In a field-cooling experiment, magnetic flux is already present in the sample as it is quenched in the mixed superconducting phase. It is thus reasonable to expect that vortices are originally disordered and that, due to their mutual interactions, undergo a local ordering process. Along this process, many dislocations annihilate, and most of the remaining dislocations arrange themselves into grain boundaries with various orientations. The growth of crystalline vortex grains is due to the motion of these separating boundaries. The resulting polycrystalline structure has been indeed observed experimentally by means of Bitter decorations of both high- [21,22] and low-T_c (Refs. 17–19 superconducting samples. The effect of quenched disorder is to pin the grain boundaries, hindering the growth process. Thus to understand the properties of vortex polycrystals, it is important to analyze the dynamics of grain boundaries in vortex matter as they interact with disorder.[40]

Grain growth is driven by a reduction in energy. For an average grain size R and straight grain boundaries, the characteristic energy stored per unit volume in the form of grain boundary dislocations is of the order of Γ_0/R, where Γ_0 is the energy per unit area of a grain boundary. Hence, the energy gain achieved by increasing the grain size by dR is $\Gamma_0/R^2 dR$. Physically, the removal of grain boundary dislocations occurs through the motion of junction points in the grain boundary network. As junction points must drag the connecting boundary with them, which may be pinned by disorder, motion can only occur if the energy gain at least matches the dissipative work which has to be done against the pinning forces. The dissipative work per unit volume expended in moving all grain boundaries by dR is $\sigma_c b/(DR)dR$, where σ_c is the pinning force per unit area. Balancing against the energy gain yields the limit grain size

$$R_g \approx \frac{D\Gamma_0}{b\sigma_c}. \tag{27}$$

An explicit expression for the grain size can be obtained by inserting σ_c, reported in Eq. (24) for the weak-pinning regime, yielding $R_g \propto R_a$. A similar calculation can be performed in the strong-pinning regime[40] and the results appear to be in good agreement with experiments measuring average grain sizes in NbMo.[16]

IV. THE EFFECT OF GRAIN BOUNDARIES ON THE CRITICAL CURRENT

Numerical simulations of interacting vortices in two dimensions (2D) allow one to verify and to keep track of the ordering process and the grain formation after a rapid field cooling of the vortex system in thin superconducting films. To this end, we consider a square 2D superconducting cross section of linear dimension L perpendicular to the external magnetic field $\mathbf{B}$ along the z direction, where we locate a set of N_v rigid vortices (for most of the results presented here, we have considered values of N_v ranging from 516 to 4128). The dynamics of each vortex line i at position $\mathbf{r}_i$ can be described by an overdamped equation of motion of the form

$$\Gamma d\mathbf{r}_i/dt = \sum_j \mathbf{f}_{vv}(\mathbf{r}_i - \mathbf{r}_j) + \sum_j \mathbf{f}_{vp}(\mathbf{r}_i - \mathbf{r}_j^p) + \mathbf{f}_L(\mathbf{r}_i), \tag{28}$$

where Γ is the effective viscosity for vortex flow. The first term on the right-hand side of this equation follows from the fact that a pair of vortices interact with each other via a long-range force $\mathbf{f}_{vv}(\mathbf{r}) = AK_1(|\mathbf{r}|/\lambda)\hat{r}$, where $A = \Phi_0^2/(8\pi^2\lambda^3)$, Φ_0 is the quantized flux carried by the vortices, λ is the London penetration length, and K_1 is a first-order modified Bessel function.[52] Distances are always measured in units of λ. The second contribution reflects the attractive interaction forces between vortex lines and quenched in point defects

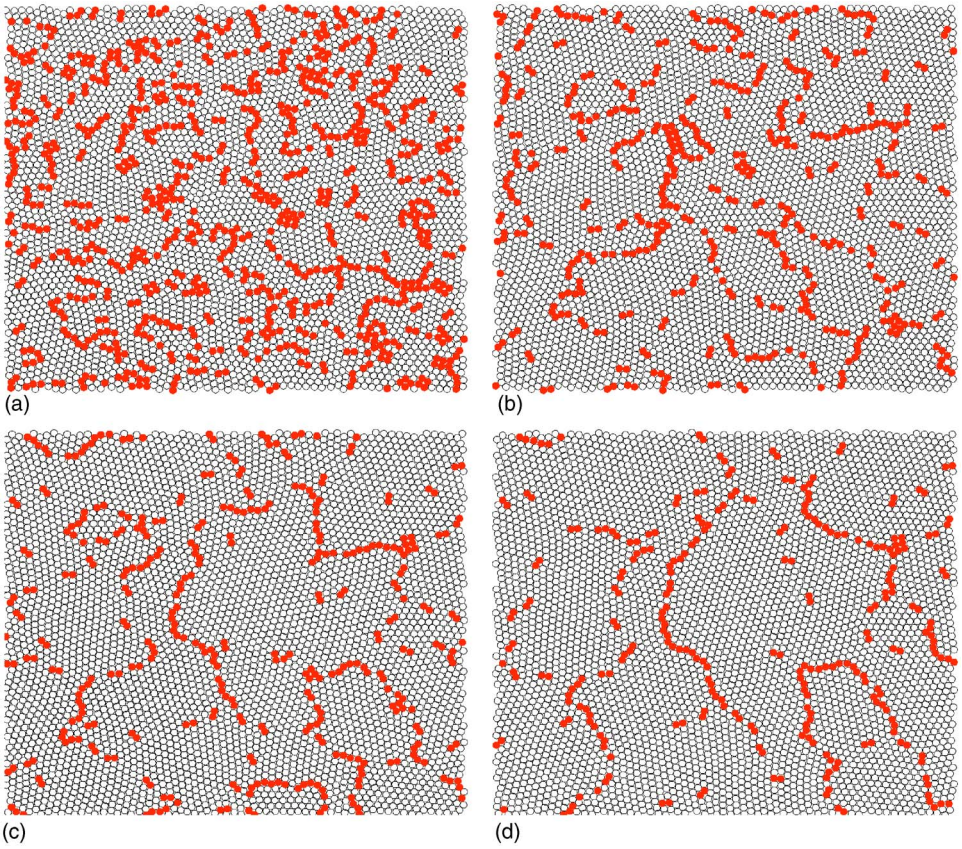

FIG. 1. (Color online) Relaxation of the topological defect structure from a simulation of $N_v = 4128$ interacting vortices after a sudden field cooling from a disordered vortex state in a simulation cell of linear size $L = 36\lambda$. The five- and sevenfold coordinated vortices (filled circles) indicate dislocations in the vortex lattice. The final configuration (d) is completely pinned by disorder. There one can observe a polycrystalline structure with most dislocations arranged into grain boundaries.

such as oxygen vacancies or other impurities in the material. These pinning centers are randomly located at positions $\mathbf{r}_i^p$ $(i=1,\ldots,N_p)$ within the simulation box, and exert pinning forces according to a Gaussian potential of the form $V(\mathbf{r}-\mathbf{r}^p)=V_0\exp[-(\mathbf{r}-\mathbf{r}^p)^2/\xi^2]$, whose amplitude and standard deviation are V_0 and ξ, the characteristic coherence length of the superconductor, respectively. (The usual number of pinning centers N_p considered is 4128, and we have chosen $\xi=0.2\lambda$, characteristic of low-temperature superconductors such as NbSe or NbMo.) Finally, if an external current $\mathbf{J}(\mathbf{r})$ is eventually applied to the sample, it generates a Lorentz-like force acting on the vortices $\mathbf{f}_L(\mathbf{r})=\Phi_0\mathbf{J}(\mathbf{r})\times\hat{z}/c$, where c is the speed of light. These coupled equations of motion (28) are numerically solved with an adaptive-step-size fifth-order Runge-Kutta algorithm, imposing periodic boundary conditions in both directions.

We first consider the relaxation dynamics of the vortex lines in the absence of driving currents. Moreover, in the present analysis we completely disregard thermal effects, that is, we mimic the dynamics of the vortex system after a sudden quench of the superconducting sample from high temperatures (or equivalently, random vortex configurations) toward the lower-energy states corresponding to zero temperature. After a transient regime, the dynamics stops due to disorder. We analyze the resulting spatial configuration of flux lines by means of Delaunay triangulations. A pair of a fivefold and a sevenfold neighboring vortex correspond to a dislocation in the vortex lattice. In the course of the simulations, the number of five- and sevenfold coordinated vortices is the same, indicating that during the relaxation process no other topological defects such as disclinations appear to be present in the lattice.

In Fig. 1, we report a series of snapshots illustrating that the gradual ordering process involves the arrangement of dislocations in grain boundaries. The formation of these walls of dislocations screens out the long-range elastic stress and strain fields otherwise created by dislocations in the lattice and, at the same time, they render a polycrystalline structure of the vortex array. This polycrystalline structure evolves in time until the residual stresses accumulated in the distorted vortex lattice drop down below the critical value σ_c. At this point, grain boundaries get pinned by disorder, limiting the average grain size [see Fig. 1(d)]. Moreover, the limit grain size R_g/a appears to increase with magnetic field $B \propto N_v$ (see Fig. 2), in qualitative agreement with experimental results[16] and the theoretical predictions reported in Ref. 40.

Different experimental, or simulation, protocols will certainly influence the relaxation dynamics and the resulting metastable configurations of trapped dislocations and grain boundaries. Metastability and history-dependent features have been long recognized in driven vortex lattices.[20] We have considered a field-cooling procedure since most of the Bitter decoration experiments are performed in a similar manner,[19,20,53] and can thus be well described by the current simulations. Nevertheless, other numerical protocols can also be devised, as for instance the one recently proposed in Ref. 36 to examine the vortex topology across the so-called peak effect, that are better suited to reproduce diverse experimental conditions.

Next, we study the behavior of the critical current $J_c(B)$ for these 2D vortex polycrystals by means of numerical

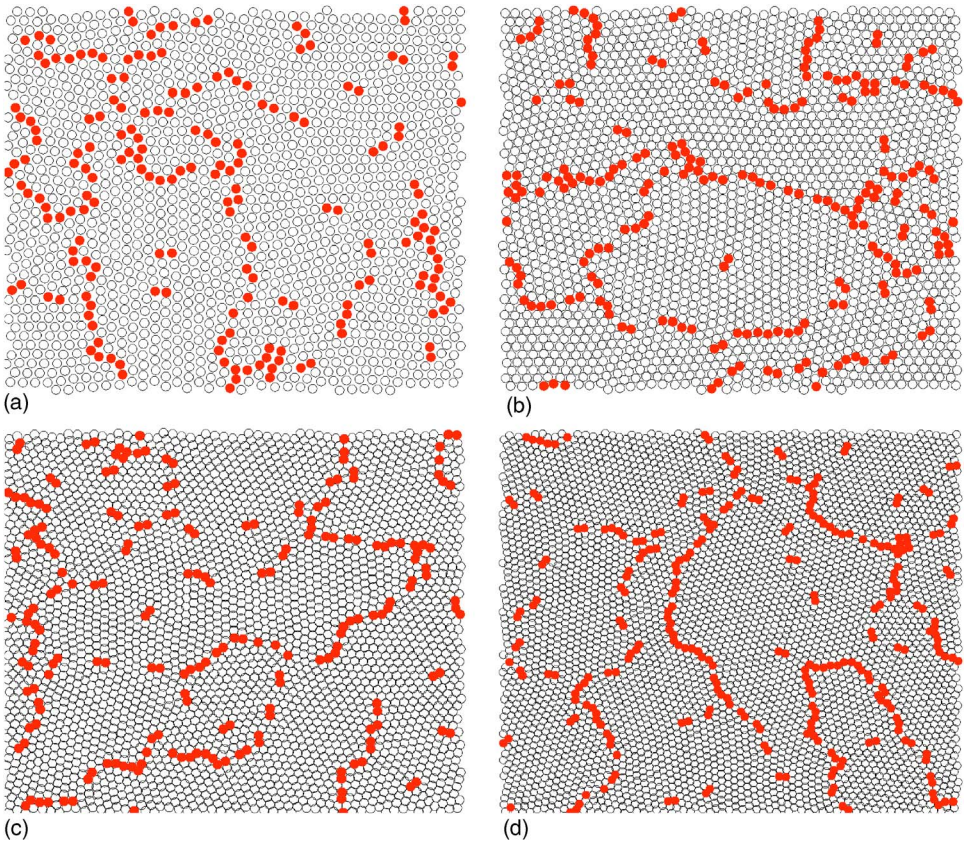

FIG. 2. (Color online) Pinned vortex structure for different values of the magnetic field: N_v=(a) 1460, (b) 2064, (c) 2919, (d) 4128, after a sudden field cooling from a disordered vortex state in a simulation cell of linear size $L=36\lambda$. The five- and sevenfold coordinated vortices (filled circles) indicate dislocations in the vortex lattice. The average grain size in the resulting polycrystalline structure seems to grow with the intensity of the average magnetic field inside the cell.

simulations. An externally applied current may induce the annealing of the metastable configurations (at least, to a certain degree that obviously depends on its intensity) present in Figs. 1 and 2. This is indeed observed in our numerical simulations, where we can as well identify the critical current J_c below which the average motion of the vortex lattice eventually ceases after a rich initial transient of plastic flow. As one can observe, for instance, in Fig. 3, a small current below the threshold value $J_c(B)$ gives rise to nontrivial (i.e., not just a slight drift along the force direction f_L^x) changes of the displacement field $\mathbf{u}_n$ of the vortex lattice. The vortex displacements are heterogeneously distributed and a small component perpendicular to the force direction can be observed. This, in turn, implies changes of the elastic shear stress distribution responsible for the Peach-Koehler forces acting on grain boundary dislocations which, as a consequence, may move and rearrange in response to the new force field.

We have determined the dependence of the critical current on the magnetic field by carrying out simulations for different densities of vortices in the simulation cell. Moreover, we have compared these results with those corresponding to a completely different initial state: a perfect single-crystal configuration with similar densities. Our results are summarized in Fig. 4. The qualitative and quantitative differences between the two curves represented in the figure are due to the presence of grain boundaries. The presence of these topological defects in the vortex configuration enhances the critical current needed to give rise to a steady regime of plastic flux flow, which in this case appears to be controlled by grain boundary motion. The plastic deformation of crystals is usually mediated by the nucleation and motion of dislocations.[49] Another possible mechanism for plastic flow is the glide motion of grain boundaries which, as in this case, can be the most relevant mechanism when the grain sizes are limited and there is a high fraction of grain boundary atoms. According to our numerical results, grain boundaries are more effi-

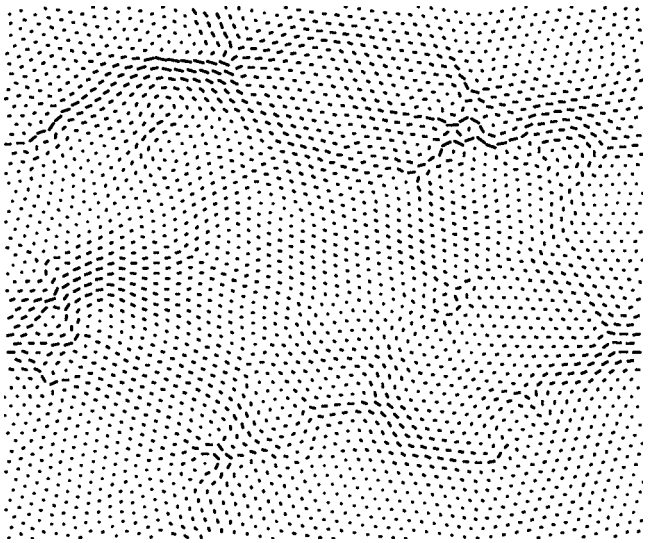

FIG. 3. Vortex trajectories between two pinned configurations obtained after the application of a small driving current below the threshold value $J_c(B)$. Small and heterogeneously distributed displacements of the vortex positions are observed in both the parallel and perpendicular directions to the applied force f_L^x. The number of vortices in the simulation cell of linear size $L=36\lambda$ is $N_v=2919$. The number of pinning points $N_p=4128$.

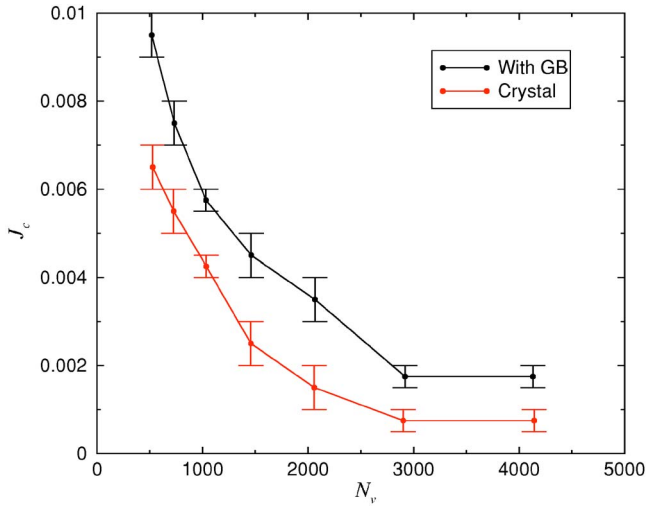

FIG. 4. (Color online) The critical current J_c as a function of the number of vortices N_v in the simulation cell. The number of pinning points N_p=4128, the cell size L=36λ, and the Ginzburg-Landau parameter considered is κ=5. The upper line shows the results obtained starting from initial field-cooled configurations containing grain boundaries (GBs), whereas the lower curve shows the numerical results obtained from perfect crystalline initial configurations.

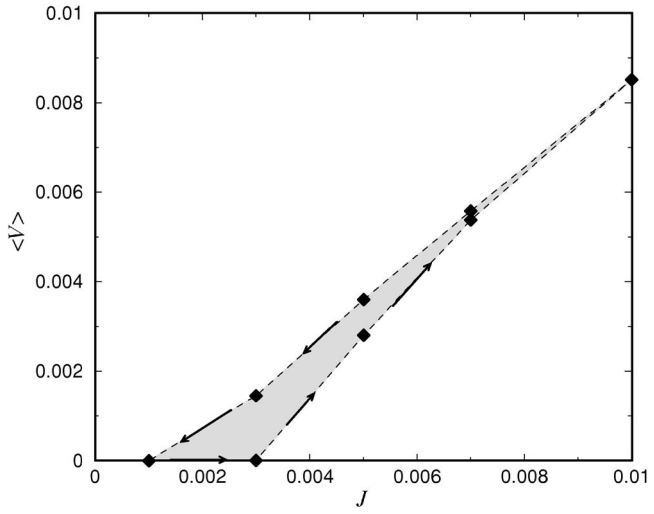

FIG. 5. The steady-state average velocity of the vortices as a function of the applied current J. The current is ramped up (and down) in steps and is kept constant after each step until the system reaches a steady state. The arrows indicate the direction of the ramp. The number of vortices is N_v=2064, the number of pinning points N_p=4128, the cell size L=36λ, and the Ginzburg- Landau parameter considered is κ=5.

ciently pinned by disorder, in agreement with the general expectation that grains adjust better to the disordered landscape than a perfectly ordered lattice. In both cases, we observe the decrease of J_c with an increasing density of vortices until this reaches a plateau for the largest number of vortices considered.

It is also worth noting that we have not considered the renormalization of either the penetration length λ or the coherence length ξ of the superconductor with the intensity of the magnetic field B. Within a mean-field scenario, these parameters should diverge as the magnetic field approaches the upper critical field $B_{c_2}=\Phi_0/2\pi\xi$. An estimation of the reduced field values we are dealing with in the simulations yields $B/B_{c_2}=2\pi N_v/(\kappa^2 L^2)\sim 0.1$–$0.8$. This means that the renormalization of λ and ξ will be especially relevant for the last point of the curves in Fig. 4. Recent simulations[36] of similar vortex lattices in 2D show that indeed such a field renormalization could be responsible for a sudden increase of the critical current close to the upper critical field B_{c_2}.

On an experimental ground, our results match, at least on a qualitative basis, the behavior exhibited by vortex matter in critical current measurements at low magnetic fields. As stated above, grain boundaries are commonly observed in field-cooled (FC) samples. On the other hand, ordered vortex crystals can be obtained in zero-field-cooling (ZFC) experiments, i.e., applying a magnetic field only after temperature has been lowered to the expected value.[10,41–46] The FC state is usually characterized by a higher critical current and has been proven to be metastable.[42,44] These aspects result in a peculiar hysteretic behavior commonly observed in critical current measurements[42,44] and I-V characteristics.[41,43] In our numerical analysis, the evaluation of critical currents in perfect vortex crystals (lower line in Fig. 4) fairly mimics the phenomenology of ZFC measurements, while results for the grain boundary model (upper line in Fig. 4) can be interpreted as a simulation of the FC response. Hysteresis is in fact reproduced by our simulations when we start from the polycrystalline state. As shown in Fig. 5, when the current J is ramped up vortices start to move at a current J_{c1}, with a velocity that then increases with the current. If the current is ramped down from the moving state, vortices get pinned at a lower value of the current J_{c2} corresponding to the critical current measured for a perfect crystal upon ramping up the field. Notice the similarity with the experimental results of Refs. 41 and 43. Once more, we should underline how these results hold only for low values of the applied field. As the magnetic induction approaches its critical value, a sudden increase in measured critical currents is observed in both the ZFC and the FC experimental setup.[42,44]

V. GRAIN-BOUNDARY-INDUCED MELTING

The stability of crystalline ordering in a vortex lattice beyond the well-known Bragg glass regime is still a matter of investigation. Experimental results suggest that an increase in temperature above a certain critical value T_m determines the transition to a *liquid* phase,[5–7] while the effects of disorder associated with high magnetic fields are responsible for the insurgence of a *glassy* phase.[8–10] A deep theoretical understanding of such transition phenomena, accounting for their microscopic origin, has not been achieved yet. Nonetheless it has been shown that for strong enough disorder the Bragg glass phase is unstable against dislocation formation.[26–28] This suggests that the melting process could be ruled by topological defects (as discussed in Ref. 30) in analogy with two-dimensional theories of crystal melting. Here we discuss the possibility that, under the effects of fluctuations, dislocations unbind and rearrange in grain

boundaries giving rise to a polycrystalline structure.[38] In this framework, the vortex polycrystal can be seen as an intermediate stage in a process that ends in the amorphous or liquid phases.

Our purpose is to study the quasiequilibrium properties of such a polycrystalline stage, using the elastic properties of grain boundaries in a vortex lattice derived in Sec. II. The main goal of our analysis is to write the free-energy density f of the system as a function of different lattice arrangements in configuration space. A minimum in free energy for a polycrystalline configuration in proximity to the melting line would corroborate the hypothesis of a grain-boundary-mediated transition. For our purposes, we parametrize configuration space in terms of linear grain boundary density n, meaning that an $n \to 0$ configuration corresponds to an ordered (grain-boundary-free) vortex lattice. Our consideration focuses on the thermally induced melting transition and the effects of impurities are neglected.

We consider arrays of edge dislocations, parallel to the z axis and arranged in low-angle grain boundaries. As in the case of grain growth, all Burgers vectors are in the xy plane, corresponding to a columnar grain structure. Following the aforementioned ideas,[38] we can introduce the linear concentration of grain boundaries n and in the low-density limit we can expand the free-energy functional (per unit volume) in powers of n as

$$f(n) = (\gamma_0 + \gamma_T)n + \Gamma n^2 - M\Gamma n^3. \tag{29}$$

The different coefficients of the expansion are explained in the following. The linear term is due to the elastic energy of grain boundaries. The zero-temperature contribution γ_0 is the elastic energy per unit surface of a flat or smooth grain boundary that, in the limit of low-angle grain boundaries, is given by[49]

$$\gamma_0 \simeq \frac{c_{66}b^2}{2\pi D}\ln\frac{e\chi D}{2\pi b}, \tag{30}$$

where the $\chi > 0$ factor takes into account core interaction effects. The γ_T term, on the other hand, accounts for thermal fluctuations. Indicating the elastic Hamiltonian in Eq. (13) as $\mathcal{H} = \int [d^2k/(2\pi)^2]\phi(\mathbf{k})X(\mathbf{k})X(-\mathbf{k})$ with $\phi(\mathbf{k}) = \epsilon|\mathbf{k}|$, and $\epsilon = \pi b^2 K/2D^2$, the partition function of a thermally perturbed grain boundary over a surface S is thus

$$\mathcal{Z} = \int \prod_{\mathbf{k}} du_{\mathbf{k}} e^{-\beta\phi_{\mathbf{k}}u_{\mathbf{k}}^2} \tag{31}$$

and the corresponding free energy per unit surface

$$\gamma_T = -\frac{1}{\beta S}\ln \mathcal{Z} \tag{32}$$

with $\beta = (k_B T)^{-1}$. The above term can be determined explicitly calculating the logarithm of the partition function as

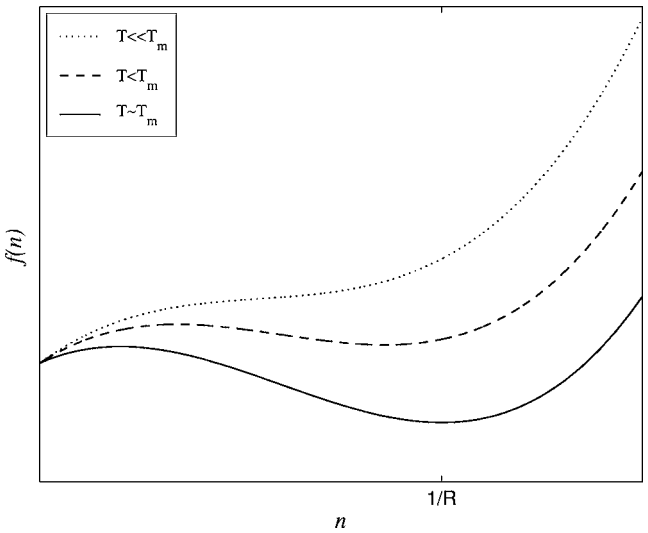

FIG. 6. Free-energy density as a function of grain boundary density close to thermal melting point.

$$\ln \mathcal{Z} = \frac{S}{2}\left[\frac{1}{Da_z}\ln\left(\frac{e^{3/2}}{2\beta\epsilon S\xi^2}\frac{Da_z}{\sqrt{D^2+a_z^2}}\right) + \frac{1}{D^2}\arctan\frac{D}{a_z} + \frac{1}{a_z^2}\arctan\frac{a_z}{D}\right] \tag{33}$$

where we have introduced a short-wavelength cutoff $2\pi/a_z$ to delimit the integration domain along the z axis.

The Γ coefficient of the n^2 term is proportional to the energy of a junction between two grain boundaries and details of its computation will be given in Appendix.

The n^3 term captures the case of the intermission of a third grain boundary in a junction, screening the effect introduced by the n^2 contribution. When this is the case, one loses an energy equal to Γn^2 times the probability of such an event. In the low-density limit, this probability is Mn, where $M = 2\pi/D$ is roughly the interaction range of a grain boundary.[38]

It is convenient to define $\Theta = \ln \mathcal{Z}/S$, so that the free-energy functional in Eq. (29) can be rewritten as

$$f(n) = k_B\Theta(T_m - T)n + \Gamma n^2 - M\Gamma n^3, \tag{34}$$

defining the melting temperature as $T_m = \gamma_0/k_B\Theta$. As shown in Fig. 6, for values of T close to T_m, $f(n)$ shows a global minimum corresponding to a GB density $1/R = [1+\sqrt{1+3K_B\Theta(T_m-T)M/\Gamma}]/3M$ where R is the average grain size. As discussed above, this suggests the possibility of a polycrystalline arrangement before the amorphous phase takes over. As soon as T reaches its melting value T_m, the global minimum density becomes of the order of D^{-1}, grains cannot be defined, and the system loses polycrystalline ordering in favor of a liquid-amorphous phase characterized by a typical dislocation spacing of order a.

The considerations above allow us to draw a phase diagram for the vortex array at low applied magnetic fields (i.e., when effects of disorder can be neglected). The resulting plot is shown in Fig. 7. The melting line is obtained plotting the

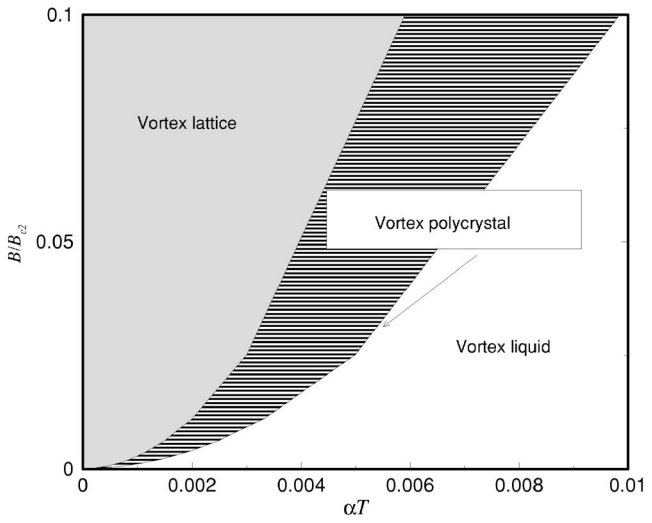

FIG. 7. Phase diagram of the vortex ensemble for low values of the reduced field B/B_{c_2}. The temperature is rescaled by the quantity $\alpha=k_B/(\xi\epsilon_0)$, where $\epsilon_0=(\Phi_0)^2/(4\pi\lambda)^2$ is an energy per unit length along the magnetic field direction, i.e., the typical energy for vortex interactions. The melting line is anticipated by the insurgence of a polycrystalline ordering.

above temperature T_m as a function of the magnetic induction. Here we use the expression for the local value of c_{66} reported in Ref. 54. The curve shows reentrant behavior expected for low fields, due to the exponential decay of the elastic shear modulus in the $B/B_{c_2}\to 0$ limit. The line delimiting lattice and polycrystal phases, instead, is obtained by imposing that the free-energy minimum shown in Fig. 6 is a global minimum. In the presence of disorder, we obviously expect modifications of this schematic phase diagram. Nevertheless, for weak enough disorder the main features should remain valid.

VI. SUMMARY AND OUTLOOK

In this paper we have investigated the properties of grain boundaries in a vortex polycrystalline phase. A vortex polycrystal is experimentally observed in field-cooling experiments when grain growth is arrested by disorder,[14,16–20] and could also arise close to the melting line as an intermediate stage between the vortex lattice and the vortex liquid or glass.[36,37] In both cases, the dynamics of the system can be studied analyzing grain boundaries, which play a similar role to that of domain walls in ferromagnetic systems. Grain boundaries can be seen as elastic manifolds whose nonlocal surface tension can be obtained from the elastic description of the vortex lattice. Deformations are due to thermal fluctuations or to random stresses induced by vortex lattice deformations.[30] Once the main ingredients (i.e., elasticity and disorder) have been properly described, grain boundaries can be studied with standard scaling methods, used in the past for various systems from flux lines to ferromagnetic domain walls. In particular, we have studied disorder-induced roughening, depinning under an applied stress, and creep. These results are important to quantify arrested grain growth due to disorder and can be used to estimate the grain size in field-cooling experiments.[40]

An important question concerns the relevance of a polycrystalline vortex structure for the transport properties of a superconductor.[20] We have shown by numerical simulations that the critical current of a vortex polycrystal is systematically higher than the one observed in the corresponding single-crystal case. This result reflects the fact that a polycrystal is pinned more effectively than a single crystal.

Finally, we have extended the theory of grain-boundary-induced melting[38] to vortex lattices. We have written the free energy as a function of the grain boundary density considering the contributions due to thermal fluctuations, elastic deformations, and junction formation. We find that the ordered crystal melts into a liquid passing through an intermediate polycrystalline phase in agreement with recent numerical results.[36,37] We have drawn a schematic phase diagram as a function of temperature and magnetic field which, however, can only be considered as a first rough approximation. We have not taken into account the effect of disorder, which is believed to be responsible for the field-induced transition to an amorphous vortex glass. In addition, we have neglected the effect of isolated dislocations and their interactions with grain boundaries. Therefore at this stage the present theory should be seen mainly as a framework for a general physical mechanism,[47] supported by simulations[36,37] and by some experiments,[48] for vortex lattice melting.

ACKNOWLEDGMENTS

We thank M. Zaiser for discussions and suggestions. This work has been partially supported by DGES of the Spanish government, Grant No. FIS2004-05923-CO2-02. M.C.M. acknowledges financial support from the Ministerio de Educacin y Ciencia (Spain) and from the Departament d'Universitats, Recerca i Societat de la Informaci, Generalitat de Catalunya (Spain).

APPENDIX: ESTIMATE OF THE ENERGY ASSOCIATED WITH JUNCTION FORMATION

The presence of an n^2 term in the free-energy functional (Ref. 29) was first suggested by Chui,[38] in order to take into account grain boundary crossing in the framework of a crystal melting theory. Such a crossing energy consisted of a thermal contribution due to coupling between fluctuations of dislocations of crossing grain boundaries. Nonetheless, Bitter decoration experiments show that in vortex polycrystals, grain boundaries primarily rearrange forming junctions, instead of simply crossing. The formation of such junctions determines variations in the overall free energy of the system due to two different contributions, a zero-temperature junction elastic energy and a thermal part related to fluctuations. In the following, we will address these contributions, respectively, as Γ_0 and Γ_T, with $\Gamma=\Gamma_0+\Gamma_T$.

Zero-temperature energy

We assume that because of the short-range nature of a grain boundary stress field, grain boundary interactions are

screened for long distances and we show that forming a junction leads to a zero-temperature elastic energy gain $\Gamma_0 \neq 0$.

The idea is to focus on what happens when two grain boundaries come so close that they can form a junction. Let us consider the first grain boundary, e.g., directed along $\mathbf{j}$ with Burgers vectors $\mathbf{b}_n$ such that $\mathbf{b}_n \cdot \mathbf{i} = b_n$, and a single dislocation, belonging to the other grain boundary, whose Burgers vector is $\mathbf{b}' \cdot \mathbf{i} = -b' \cos\varphi$, φ being the junction angle.

Since grain boundary interactions are short ranged, we expect misorientation effects to make no difference in the energy computation until dislocations come close to a distance that we will call $\bar{s}$. If, on a distance $\bar{s}$, the interaction energy for $\varphi = 0$ is lower than for $\varphi \neq 0$, there in no reason for the system to make a junction. Otherwise, if there is an energy gain, grain boundaries are likely to join.

Considering the general expression for dislocation interactions

$$V = -\frac{K}{2\pi}\left[\ln\frac{e\alpha|\mathbf{r}-\mathbf{r}'|}{b}\mathbf{b}\cdot\mathbf{b}' - \frac{\mathbf{b}'\cdot(\mathbf{r}-\mathbf{r}')\mathbf{b}\cdot(\mathbf{r}-\mathbf{r}')}{|\mathbf{r}-\mathbf{r}'|^2}\right], \tag{A1}$$

where $\mathbf{r}$ and $\mathbf{r}'$ are the positions of interacting dislocations, the energy (per unit length) of our system (GB and rotated dislocation) is

$$E_s(\varphi) = \frac{Kb^2}{4\pi}\left[\left(\sum_{n=-\infty}^{+\infty}\ln\frac{e^2\alpha^2(s^2+n^2D^2)}{b^2} - 2\sum_{n=-\infty}^{+\infty}\frac{s^2}{s^2+n^2D^2}\right)\times\cos\varphi - \left(\sum_{n=-\infty}^{+\infty}\frac{snD}{s^2+n^2D^2}\right)\sin\varphi\right], \tag{A2}$$

where s is the distance between the rotated dislocation and the grain boundary. Moreover, after summing the series,

$$E_s(\varphi) = \frac{Kb^2}{2\pi}\left[\ln\left(\frac{e\alpha D}{\pi b}\sinh\frac{\pi s}{D}\right) - \frac{\pi s}{D}\coth\frac{\pi s}{D}\right]\cos\varphi. \tag{A3}$$

Assuming that we have M dislocations within the range of $\bar{s}$, the energy gain due to a junction will be

$$\Gamma_0 = \sum_{m=1}^{M} E_{s_m}(\varphi) - ME_{\bar{s}}(0) < 0. \tag{A4}$$

Since the stress field generated by a grain boundary is exponentially suppressed beyond a distance of the same order of the dislocation spacing, we can give a rough estimate of the sum taking $M=1$ and $s_1 = D$, i.e.,

$$\Gamma_0 \simeq -\frac{Kb^2}{2\pi}(1-\cos\varphi)\ln\left(\frac{e\alpha D}{2\pi b}\right). \tag{A5}$$

Thermal fluctuations

The Γ_T contribution, due to the coupling between fluctuations of dislocations belonging to different grain boundaries in a junction, can also be estimated following Ref. 38. After performing the thermal average of the interaction potential (A1), calculated on the cylinder of radius $|r| < (2/\sqrt{3})D/\pi$ and taking the short-range logarithmic part of V

$$\Gamma_T = \mathcal{N}\int dz \int_A dr\, rV\, e^{-\beta V}, \tag{A6}$$

$\mathcal{N}$ being a normalization constant. Evaluating the integral for $T \simeq T_m$ leads to

$$\Gamma_T \simeq -\frac{Kb^2}{2\pi}\cos\varphi\ln^2\left(\frac{D}{b}\frac{2}{\pi\sqrt{3}}\right), \tag{A7}$$

where φ is the average junction angle. In the estimate of the lattice-polycrystal crossover we have assumed $\varphi \simeq \pi/3$, as is often observed in decoration experiments.

[1] G. Blatter, M. V. Feigel'man, V. B. Geshkenbein, A. I. Larkin, and V. M. Vinokur, Rev. Mod. Phys. **66**, 1125 (1994).

[2] E. H. Brandt, Rep. Prog. Phys. **58**, 1465 (1995).

[3] T. Giamarchi and S. Bhattacharya, in *High Magnetic Fields: Applications in Condensed Matter Physics and Spectroscopy*, edited by C. Berthier *et al.* (Springer-Verlag, Berlin, 2002), p. 314.

[4] A. A. Abrikosov, Zh. Eksp. Teor. Fiz. **32**, 1442 (1957).

[5] H. Safar, P. L. Gammel, D. A. Huse, D. J. Bishop, J. P. Rice, and D. M. Ginsberg, Phys. Rev. Lett. **69**, 824 (1992).

[6] F. Bouquet, C. Marcenat, E. Steep, R. Calemczuk, W. K. Kwok, U. Welp, G. W. Crabtree, R. A. Fisher, N. E. Phillips, and A. Schilling, Nature (London) **411**, 448 (2001).

[7] N. Avraham, B. Khaykovich, Y. Myasoedov, M. Rappaport, H. Shtrikman, D. E. Feldman, T. Tamegai, P. H. Kes, M. Li, M. Konczykowski, K. van der Beek, and E. Zeldov, Nature (London) **411**, 451 (2001).

[8] R. Cubitt, E. M. Forgan, G. Yang, S. L. Lee, D. McK. Paul, H. A. Mook, M. Yethiraj, P. H. Kes, T. W. Li, A. A. Menovsky, Z. Tarnawski, and K. Mortensen, Nature (London) **365**, 407 (1993).

[9] P. L. Gammel, U. Yaron, A. P. Ramirez, D. J. Bishop, A. M. Chang, R. Ruel, L. N. Pfeiffer, E. Bucher, G. D'Anna, D. A. Huse, K. Mortensen, M. R. Eskildsen, and P. H. Kes, Phys. Rev. Lett. **80**, 833 (1998).

[10] X. S. Ling, S. R. Park, B. A. McClain, S. M. Choi, D. C. Dender, and J. W. Lynn, Phys. Rev. Lett. **86**, 712 (2001).

[11] D. S. Fisher, M. P. A. Fisher, and D. A. Huse, Phys. Rev. B **43**, 130 (1991).

[12] D. R. Nelson and V. M. Vinokur, Phys. Rev. B **61**, 5917 (2000).

[13] T. Giamarchi and P. Le Doussal, Phys. Rev. Lett. **72**, 1530 (1994).

[14] I. V. Grigorieva, Supercond. Sci. Technol. **7**, 161 (1994).

[15] U. Essmann and H. Trauble, Phys. Lett. **56A**, 596 (1967).
[16] I. V. Grigorieva, Sov. Phys. JETP **69**, 194 (1989).
[17] M. V. Marchevsky, Ph.D. thesis, Leiden University, 1997.
[18] M. Marchevsky, A. Keurentjes, J. Aarts, and P. H. Kes, Phys. Rev. B **57**, 6061 (1998).
[19] Y. Fasano, M. Menghini, F. de la Cruz, Y. Paltiel, Y. Myasoedov, E. Zeldov, M. J. Higgins, and S. Bhattacharya, Phys. Rev. B **66**, 020512(R) (2002).
[20] F. Pardo, F. De La Cruz, P. L. Gammel, C. S. Oglesby, E. Bucher, B. Batlogg, and D. J. Bishop, Phys. Rev. Lett. **78**, 4633 (1997).
[21] H. Dai, J. Liu, and C. M. Lieber, Phys. Rev. Lett. **72**, 748 (1994).
[22] J. A. Herbsommer, G. Nieva, and J. Luzuriaga, Phys. Rev. B **62**, 678 (2000).
[23] A. I. Larkin, Sov. Phys. JETP **31**, 784 (1970).
[24] T. Giamarchi and P. Le Doussal, Phys. Rev. B **52**, 1242 (1995).
[25] T. Klein, I. Joumard, S. Blanchard, J. Marcus, R. Cubbit, T. Giamarchi, and P. Le Doussal, Nature (London) **413**, 404 (2001).
[26] D. Carpentier, P. Le Doussal, and T. Giamarchi, Europhys. Lett. **35**, 379 (1996).
[27] J. Kierfeld, T. Nattermann, and T. Hwa, Phys. Rev. B **55**, 626 (1997).
[28] D. S. Fisher, Phys. Rev. Lett. **78**, 1964 (1997).
[29] G. P. Mikitik and E. H. Brandt, Phys. Rev. B **68**, 054509 (2003).
[30] J. Kierfeld and V. Vinokur, Phys. Rev. B **61**, R14928 (2000).
[31] F. R. N. Nabarro and A. T. Quintanilha, in *Dislocations in Solids*, edited by F. R. N. Nabarro (North-Holland, Amsterdam, 1980), Vol. 5.
[32] E. H. Brandt, Phys. Rev. B **34**, 6514 (1986).
[33] M. C. Miguel and M. Kardar, Phys. Rev. B **56**, 11903 (1997).
[34] J. Kierfeld, H. Nordborg, and V. M. Vinokur, Phys. Rev. Lett. **85**, 4948 (2000).
[35] M.-C. Miguel and S. Zapperi, Nat. Mater. **2**, 477 (2003).
[36] M. Chandran, R. T. Scalettar, and G. T. Zimanyi, Phys. Rev. B **69**, 024526 (2004).
[37] C. Dasgupta and O. T. Valls, Phys. Rev. Lett. **91**, 127002 (2003); Phys. Rev. B **69**, 214520 (2004).
[38] S. T. Chui, Phys. Rev. B **28**, 178 (1983).
[39] P. Moretti, M.-C. Miguel, M. Zaiser, and S. Zapperi, Phys. Rev. B **69**, 214103 (2004).
[40] P. Moretti, M.-C. Miguel, M. Zaiser, and S. Zapperi, Phys. Rev. Lett. **92**, 257004 (2004).
[41] Z. L. Xiao, E. Y. Andrei, P. Shuk, and M. Greenblatt, Phys. Rev. Lett. **86**, 2431 (2001).
[42] W. Henderson, E. Y. Andrei, M. J. Higgins, and S. Bhattacharya, Phys. Rev. Lett. **77**, 2077 (1996).
[43] Z. L. Xiao, E. Y. Andrei, P. Shuk, and M. Greenblatt, Phys. Rev. Lett. **85**, 3265 (2000).
[44] S. S. Banerjee, N. G. Patil, S. Ramakrishnan, A. K. Grover, S. Bhattacharya, G. Ravikumar, P. K. Mishra, T. V. Chandrasekhar Rao, V. C. Sahni, and M. J. Higgins, Appl. Phys. Lett. **74**, 126 (1999).
[45] I. Joumard, T. Klein, J. Marcus, and R. Cubitt, Physica C **341-348**, 2131 (2000).
[46] B. Sas, F. Portier, K. Vad, B. Keszei, L. F. Kiss, N. Hegman, I. Puha, S. Meszaros, and F. I. B. Williams, Phys. Rev. B **61**, 9118 (2000).
[47] G. I. Menon, Phys. Rev. B **65**, 104527 (2002); Mod. Phys. Lett. B **15**, 1023 (2001).
[48] U. Divakar, A. J. Drew, S. L. Lee, R. Gilardi, J. Mesot, F. Y. Ogrin, D. Charalambous, E. M. Forgan, G. I. Menon, N. Momono, M. Oda, C. D. Dewhurst, and C. Baines, Phys. Rev. Lett. **92**, 237004, (2004).
[49] J. P. Hirth and J. Lothe, *Theory of Dislocations* (Wiley, New York, 1982).
[50] A. I. Lar'kin and Yu. N. Ovchinnikov, J. Low Temp. Phys. **34**, 409 (1979).
[51] P. M. Hazzledine and R. D. J. Oldershaw, Philos. Mag. A **61**, 579 (1990).
[52] P.-G. de Gennes, *Superconductivity of Metals and Alloys* (Benjamin, New York, 1966).
[53] M. Menghini, Y. Fasano, and F. de la Cruz, Phys. Rev. B **65**, 064510 (2002).
[54] M.-C. Miguel and M. Kardar, Phys. Rev. B **62**, 5942 (2000).